

Instrument Description: The Total Solar Irradiance Monitor on the FY-3C Satellite, an Instrument with a Pointing System

Hongrui Wang^{1,2} · Yupeng Wang¹ · Xin Ye¹ ·
Dongjun Yang¹ · Kai Wang¹ · Huiduan Li³ · Wei Fang¹

Received: 16 January 2015 / Accepted: 7 November 2016 / Published online: 12 December 2016
© Springer Science+Business Media Dordrecht 2016

Abstract The *Total Solar Irradiance Monitor* (TSIM) onboard the nadir *Feng Yun-3C* (FY-3C) satellite provides measurements of the total solar irradiance with accurate solar tracking and sound thermal stability of its heat sink. TSIM/FY-3C mainly consists of the pointing system, the radiometer package, the thermal control system, and the electronics. Accurate solar tracking is achieved by the pointing system, which greatly improves the science data quality when compared with the previous TSIM/FY-3A and TSIM/FY-3B. The total solar irradiance (TSI) is recorded by TSIM/FY-3C about 26 times each day, using a two-channel radiometer package. One channel is used to perform routine observation, and the other channel is used to monitor the degradation of the cavity detector in the routine channel. From the results of the ground test, the incoming irradiance is measured by the routine channel (AR1) with a relative uncertainty of 592 ppm. A general description of the TSIM, including the instrument modules, uncertainty evaluation, and its operation, is given in this article.

1. Introduction

Accurate long-time data series of the total solar irradiance (TSI) are essential to distinguish natural solar forcing from human-induced factors or natural factors for an investigation of

This article is a companion of the article available at doi:[10.1007/s11207-016-1027-6](https://doi.org/10.1007/s11207-016-1027-6).

Electronic supplementary material The online version of this article (doi:[10.1007/s11207-016-1026-7](https://doi.org/10.1007/s11207-016-1026-7)) contains supplementary material, which is available to authorized users.

✉ W. Fang
tsim01@sina.com

¹ Changchun Institute of Optics, Fine Mechanics and Physics, Chinese Academy of Sciences, Dong Nanhu Road 3888, Changchun 130033, China

² Physikalisches-Meteorologisches Observatorium Davos, World Radiation Center, Dorfstrasse 33, 7260 Davos Dorf, Switzerland

³ Chuxiong Normal University, Lu Cheng Nan Road 546, Chuxiong 675000, China

climate change (Fröhlich, 2012; Kopp and Lean, 2011). The TSI has been recorded on several spacecraft for about four decades since 1978, providing nearly overlapping continuous measurements (Kopp *et al.*, 2012; Meftah *et al.*, 2014a).

The measurement modes of TSI instruments are impacted by the attitude-control system of the spacecraft. For TSI instruments onboard nadir-pointing spacecraft, the Sun is generally observed in a scanning manner, such as for the TSI experiments onboard the FY-3A and FY-3B satellites (Fang *et al.*, 2014; Wang *et al.*, 2015). As most payloads are developed for Earth observing (EO), the vehicle axis of each FY-3 satellite is aligned with a nadir reference, using a three-axis-stabilized system (Yang *et al.*, 2012).

The previous *Total Solar Irradiance Monitor* (TSIM) instruments had no pointing systems, such as TSIM/FY-3A and TSIM/FY-3B. Consequently, they measured the solar activity in a scanning manner (Wang *et al.*, 2015). The Sun was only observed when the satellite flew near the northern pole of the Earth, and the sunlight swept through the TSIM field of view (FOV). The time left to observe the Sun in the scanning manner was quite short. This time was no more than ten minutes for each 110-minute orbit for FY-3B/TSIM. Complex corrections for solar pointing errors are needed to obtain the TSI data products for TSIM/FY-3B, requiring complicated computations based on astronomical algorithms and satellite orbit data.

The disadvantage of the scanning manner is removed when the spacecraft have accurate solar pointing, such as the *Solar and Heliospheric Observatory* (SOHO) spacecraft for the *Variability of Solar Irradiance and Gravity Oscillations* (VIRGO) experiment (Fröhlich *et al.*, 1995), the *Solar Radiation and Climate Experiment* (SORCE) spacecraft for the *Total Irradiance Monitor* (TIM) experiment (Kopp and Lawrence, 2005; Kopp, Heuerman, and Lawrence, 2005), the *PICARD* satellite for the *Solar Variability Picard* (SOVAP) and *PREcision Monitor Sensor* (PREMOS) experiments (Meftah *et al.*, 2014a, 2014b). Longer observation time and sound solar pointing are achieved in this way for Sun measurements compared with the scanning manner. It seems that there are fewer solar observing missions than the numerous EO missions (Liu and Ofman, 2014; Morrill, Floyd, and McMullin, 2014; Wieman, Didkovsky, and Judge, 2014), especially in countries without solar-dedicated space missions. TSI instruments with pointing systems are developed for spacecraft that are mainly dedicated to EO, such as the *Solar Variability Irradiance Monitor* (SOVIM) onboard the *International Space Station* (ISS) (Mekaoui *et al.*, 2010) in the SOLAR package, and TSIM onboard the FY-3C satellite. The Coarse Pointing Device (CPD) provided the solar pointing for the spectral instrument in the SOLAR package onboard ISS (Thuillier *et al.*, 2014a, 2014b). However, due to failures in its power module, SOVIM in the same SOLAR package could not obtain solar observations with accurate solar pointing.

The pointing system of TSIM/FY-3C is expected to run in visual servo mode as long as possible. In the visual servo mode, accurate solar tracking is achieved by a nonlinear controller using image-based feedback of solar pointing errors with high resolution.

The TSI has been recorded daily since October 2013 by TSIM with nearly zero solar pointing onboard the satellite FY-3C. The pointing system works well in the closed-loop mode. TSIM/FY-3C tracks the Sun for about 15 minutes in each orbit. The TSIM/FY-3C obtains more accurate measurements than the previous TSIM instruments. Non-zero solar pointing errors and the related complex corrections are removed by the accurate pointing of the pointing system.

TSIM/FY-3C was developed by the Changchun Institute of Optics, Fine Mechanics and Physics (CIOMP) for China Meteorological Administration (CMA). It should be noted here that the TSIM is called *Solar Irradiance Monitor* (SIM) in CMA documents and data sites.

2. Instrument Concepts

The ground spare of TSIM/FY-3C is shown in Figure 1. Figure 2 presents a schematic of the instrument assembly. The TSIM/FY-3C instrument parameters are presented in Table 1.

A schematic of the instrument is shown in Figure 3. TSIM/FY-3C comprises four modules: the radiometer package, the pointing system, the thermal control system, and the electronics.

The radiometer package consists of two electrical substitution radiometers, AR1 and AR2. Radiometers AR1 and AR2 are pointed toward the Sun by the pointing system based on a feedback control principle.

FY-3C is in a Sun-synchronous polar orbit satellite with an altitude of 831 km and an inclination 98.81 deg. The orbital period is about 110 minutes and the descending node local time is 10:00 am.

The instrument of TSIM/FY-3C is installed at the +X top side of the satellite, with its opening parallel to the satellite flying direction. The cold background of the space will be seen by the instrument for about 40 minutes during the 110 minutes of satellite orbit.

Figure 1 A photograph of the new TSIM including a pointing system. The instrument in this picture is not the flight product, but the ground spare.

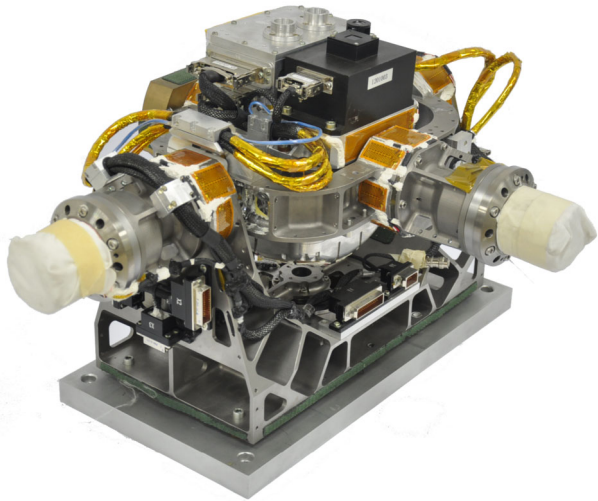


Figure 2 Computer-aided design of the TSIM/FY-3C assembly. The optical axis of the radiometer package is pointed toward the Sun by the pointing system using the motion of the pitch motor and the yaw motor. The pitch motor or yaw motor is driven to move by a visual servo controller, using high-resolution feedback provided by the sun sensor. The pointing system is fixed by a locking unit to survive the launching conditions.

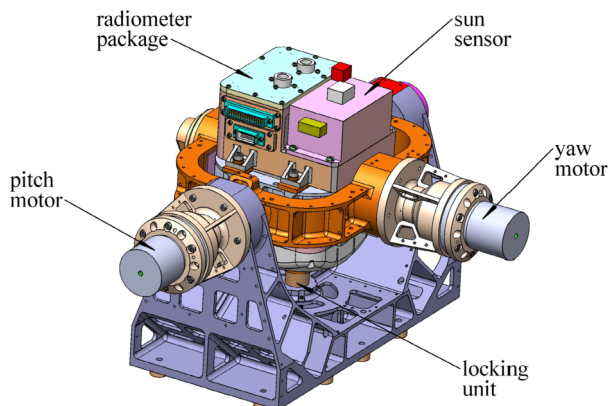


Table 1 Instrument parameters of TSIM/FY-3C.

Design lifetime	5 years
Field of view (FOV)	2°
Solar pointing error	≤ 0.1°
Effective absorption coefficient of primary cavity	0.9997
Requirement of power consumption	≤ 51 W
Instrument dimensions	576.5 mm × 450 mm × 345 mm
Instrument mass	31 kg
Electronics dimensions	301 mm × 205 mm × 234 mm
Electronics mass	11 kg
Pitch rotation range of the pointing system	80° – 140°
Yaw rotation range of the pointing system	–17° – –37°

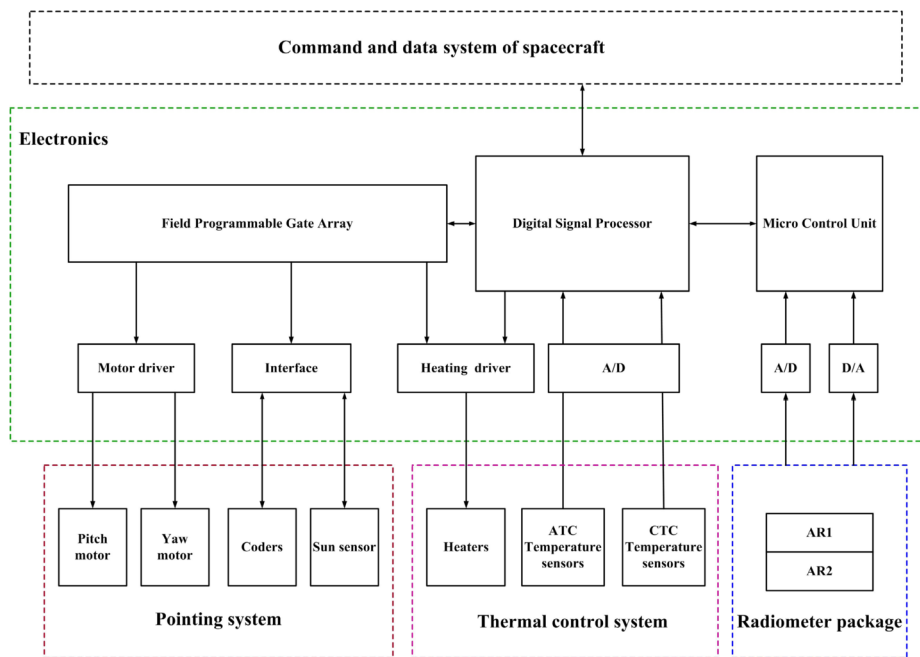
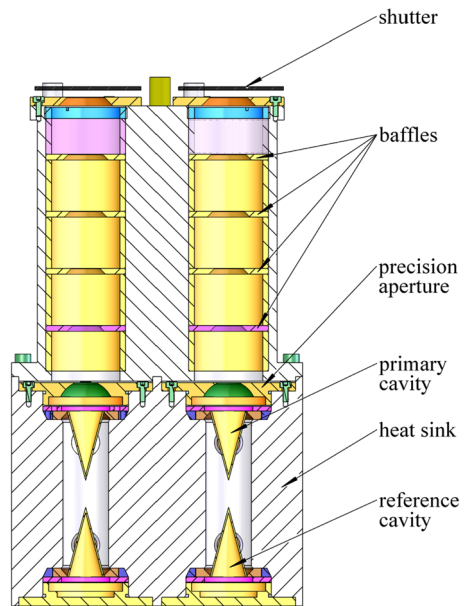


Figure 3 Schematic of the instrument system. The instrument includes the pointing system, the thermal control system, and the radiometer package. The instrument is mounted on the +X top side of the satellite outside the spacecraft, while the electronics is located inside the spacecraft. CTC is the abbreviation of coarse temperature control, and ATC is the abbreviation of accurate temperature control.

3. Radiometer Package

The design of AR1 and AR2 comes from previous radiometers in TSIM/FY-3B (Fang *et al.*, 2014; Wang, Li, and Fang, 2014). The primary cavity and the reference cavity in TSIM are not arranged in the side-by-side style proposed for the *Differential Absolute RADIometer* (DIARAD) and further improved for the TIM/SORCE. The reference cavity of TSIM/FY-3C is placed behind the primary cavity and is not exposed to any sunlight, as shown in Figure 4.

Figure 4 Schematic of the radiometer package in TSIM/FY-3C. Some flight design of TSIM/FY-3C comes from TSIM/FY-3B. The general optical layout of the radiometers in TSIM/FY-3C remains the same as in TSIM/FY-3B. Critical components of the radiometer package are developed with the same method and nearly the same materials, such as the primary cavity and the precision aperture. However, the FOV of the radiometers in TSIM/FY-3C is much smaller than in the previous TSIM to suppress stray light.



A silver cone cavity is used as the primary cavity to transfer the sunlight energy into thermal energy. The temperature difference between the primary cavity and the heat sink that is due to the thermal energy is converted into weak voltage signals by a ring of thermocouples. The silver cone cavity and the ring of thermocouples were developed using the same method as in the previous TSIM/FY-3B, with nearly the same materials and components, such as the absorptive black paints, heating wires, *etc.* As the design of the cavity sensor is not changed, the TSI is measured by TSIM/FY-3C as slowly as by TSIM/FY-3B. TSIM/FY-3C needs ten minutes to establish a single TSI measurement in its routine mode. The measurement time of TSIM/FY-3C is much longer than that of the radiometers in VIRGO/SOHO and TIM/SORCE. A cavity detector with smaller timing parameters will be developed by CIOMP for the future TSIM missions to have a faster time response.

The radiometer package has two channels. One channel is used to record the TSI daily; this is referred to as the routine channel. The other channel is used to monitor the degradation in the sensor of the routine channel (BenMoussa *et al.*, 2013); this is referred to as the backup channel.

The radiometer package is pointed toward the Sun with nearly zero pointing error, therefore the FOV of AR1 or AR2 for TSIM/FY-3C is reduced to two degrees in system design (Liebtraut *et al.*, 2013; Memarian and Eleftheriades, 2013; Witte *et al.*, 2014). Two advantages have been brought to TSIM/FY-3C by the design of a smaller FOV. Less stray light from other components of the satellite is allowed to pass through the optical system to enter the cavity detector. The radiation exchange term between the radiometer and the space background is reduced to about 10 % of that in TSIM/FY-3B (Fang *et al.*, 2014; Wang, Li, and Fang, 2014). The quality of TSI remote-sensing data will be improved by these two advantages.

A lower TSI value was reported by Kopp and Lean (Kopp and Lean, 2011), which was attributed to the optical layout of the instrument. However, the aperture arrangements of the radiometers AR1 and AR2 inside TSIM/FY-3C are not changed (Booth, 2014; Girshovitz and Shaked, 2014). The optical layout of the radiometers for TSIM/FY-3C

is similar to that of TSIM/FY-3B. The view-limiting aperture and the blackened baffles are still located in front of the precision aperture in TSIM/FY-3C. We wish to compare data of TSIM/FY-3A, TSIM/FY-3B, and TSIM/FY-3C by using the same optical layout of the radiometers. The radius of the precision apertures for TSIM/FY-3C is the same as in TSIM/FY-3B in system design (Fang *et al.*, 2014; Wang, Li, and Fang, 2014). The precision apertures for TSIM/FY-3C were developed with the same procedures and machines.

The incoming sunlight is measured by the two radiometers through the observation phase and the reference phase. In the observation phase for a single TSI measurement, the shutter of the radiometer AR1 or AR2 is open and the primary cavity is heated by the incoming sunlight. The temperature of the primary cavity is always expected to be stabilized at a constant value T_0 . In the reference phase, the shutter of the radiometer is closed and the primary cavity is heated by the electrical power alone. The electrical power is tuned to stabilize the temperature of the primary cavity again at T_0 .

The absorbed radiant power of the cavity detector in the observation phase is

$$P_s = EA\alpha \cos \beta, \quad (1)$$

where E is the TSI, A is the area of the precision aperture, α is the effective absorption coefficient of the primary cavity, and β is the solar pointing error.

The estimation method of the required electrical power in both phases, observation and the reference, is exactly the same as for TSIM/FY-3B.

4. Electronics

The electronics of TSIM/FY-3C consists of several printed circuit boards, including three large-scale integrated circuits (IC) and external circuits. The three large-scale ICs inside the electronics are a Micro Controller Unit (MCU), a Field Programmable Gate Array (FPGA), and a Digital Signal Processor (DSP). The interconnections among the instrument electronics and the instrument mechanical or optical components are summarized in Figure 3.

The electronics of TSIM/FY-3C is developed based on the heritage and past space experiences of TSIM/FY-3A and TSIM/FY-3B (Fang *et al.*, 2014; Wang, Li, and Fang, 2014). The DSP has sufficient processing capability and external interfaces to replace the MCU. However, considering the stable performance of TSIM/FY-3B in the space experiment, the MCU still performs electrical substitution measurements of the TSI. The electronics in TSIM/FY-3C for the electrical substitution of the TSI is nearly the same as in TSIM/FY-3B, such as the analog/digital (A/D) converter for temperature sensing, the digital/analog converter (D/A) for electrical heating, and the drivers for shutter motors.

All control algorithms are implemented in the DSP, such as temperature regulation for the instrument thermal control and nonlinear control for the solar tracking. The DSP also performs temperature sensing for the instrument thermal control, heater driving for coarse temperature control, and communication with the command and data system of the satellite. Commands and control instructions via telemetry links from the flight computer are handled by the DSP module. Science data produced by the instrument are handled by the DSP module and transferred to the flight computer.

Most complex tasks are performed by the FPGA module, including generating control signals for accurate temperature regulation of the heat sink in the radiometer package, driving control for instrument heaters, and motor driving control for the solar tracking with H-bridge circuit. In addition, the FPGA serves as the data interface between the DSP and other devices or external elements, such as the MCU, the sun sensor, and the coders.

5. Pointing System

The pointing system for TSIM/FY-3C includes the yaw subsystem, the pitch subsystem, a digital sun sensor, and a mechanical module, as shown in Figures 2 and 5. The pointing system is driven to rotate around its pitch axis or yaw axis to achieve two degrees of freedom (DOFs) for solar tracking. The pointing system of the TSIM follows the Sun using a scheme of visual servo. The Sun motion, the satellite orbital motion, and the orbital drift are simultaneously compensated by the two rotation DOF of the pointing system around its pitch axis and yaw axis. The optical axis of the radiometer package is accurately pointed toward the Sun through nonlinear position control of the pitch subsystem and the yaw subsystem.

In order to withstand vibrations during the launch phase, the two rotational DOF of the pointing system are fixed by a locking unit to keep them steady. The locking unit is a one-shot device, as a release mechanism. When the TSIM is considered to be ready to operate in space, an electro-explosive component inside the locking unit is fired, and the yaw DOF and pitch DOF are released to move freely in their respective limited scopes.

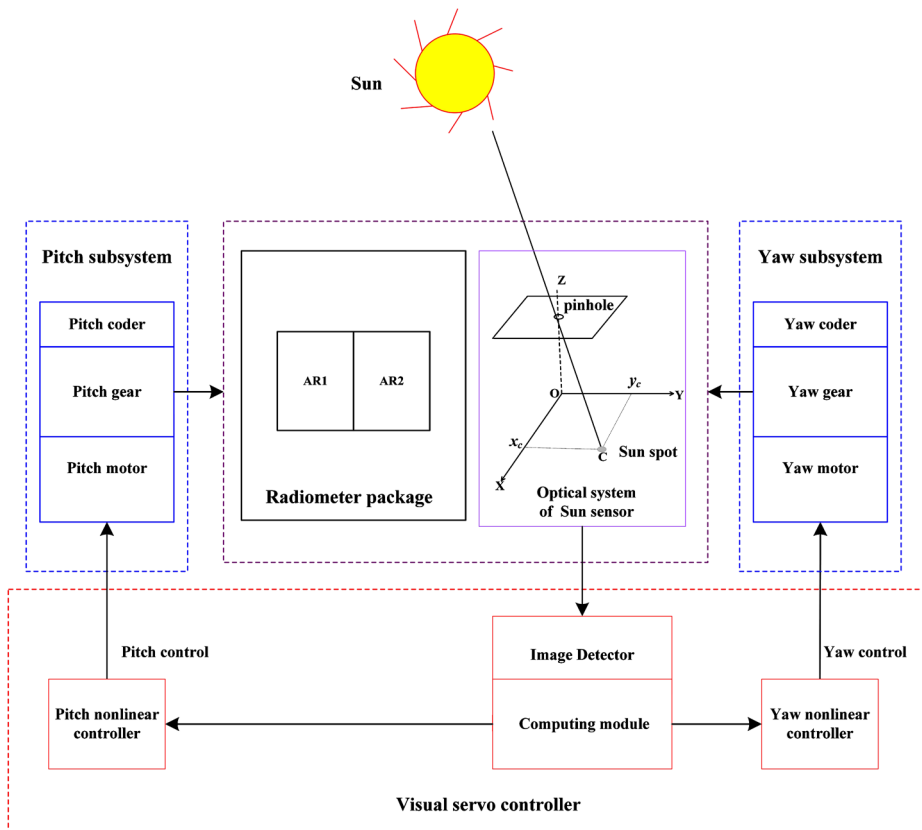


Figure 5 Visual servo controller to follow the Sun. In the routine mode, the pointing system is regulated to follow the Sun by the visual servo controller using image-based feedback provided by the digital sun sensor. The digital sun sensor has a design without lenses for simplicity and reliability. An image sensor is used in the digital sun sensor as detector.

Solar pointing errors are provided by the digital sun sensor. The solar pointing error in the pitch direction or in the yaw direction is solved using a technique of image processing based on the grabbed solar image. No lenses are used in the digital sun sensor (Yu *et al.*, 2014). This design without lenses results in huge benefits for system reliability, compactness, and robustness in space. The digital sun sensor includes an optical system with a single round aperture, an image sensor (Cetin *et al.*, 2014), and a compute module, as shown in Figure 5.

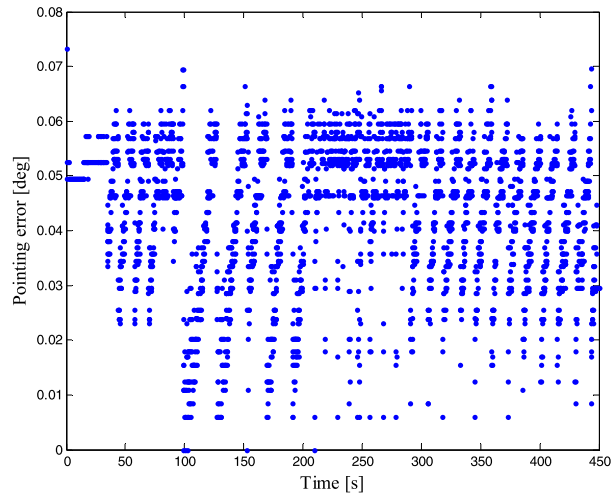
The pointing system takes an image-based feedback from the digital sun sensor as the control input to drive the pitch motor and the yaw motor to track the Sun in its routine mode, the visual servo mode. Redundant operation modes rather than the visual servo mode were defined for the pointing system to achieve better system reliability. When the image-based feedback provided by the digital sun sensor is not available, the pointing system will not run any longer in the closed-loop manner as defined in the visual servo mode. The pointing system will switch to one of the two redundant operation modes. In the first redundant operation mode, the Sun position is computed in the geocentric equatorial frame using an astronomical algorithm. In the second redundant operation mode, the Sun position is obtained using information from the sun sensors of the satellite. When the Sun position is known, it is transformed to the pointing system frame through coordinate transformation. Finally, the pitch motor and the yaw motor are driven to move to follow the estimated Sun position determined by the astronomical algorithm or provided by the satellite.

Most of the payload for Earth observing is installed on the +Z side of the FY-3C satellite. The +Z axis is always accurately pointed toward Earth by the attitude-control system of the spacecraft. The TSIM is installed on the +X top surface of the satellite near a large expanding component of a microwave instrument. The flying direction is parallel to the +X axis of the satellite. This large expanding component extends in space and is larger than TSIM/FY-3C. As a result, the instrument has only a constrained FOV of the Sun when the satellite flies out of the eclipsed portion near the North Pole of the Earth. Since the Sun could only be observed in a narrow window, it seems a waste of budget and time to design and construct a pointing system with a wider rotating range than the current one. The pointing system of TSIM/FY-3C rotates on the topside of the satellite in a constrained range as given in Table 1. The constrained rotation range of the pointing system is determined through computation and simulation of the sunlight angle in the frame of the pointing system. As shown in Table 1, the pitch subsystem is only able to rotate in a constrained range of 60 degrees, and the yaw subsystem is only able to rotate in a constrained range of 20 degrees.

According to the space experiment results, the time left for the pointing system to follow the Sun is no more than 20 minutes for each orbit as soon as the satellite leaves the eclipsed portion. However, the narrow Sun window is critical for TSIM/FY-3C to get the sunlight nearly parallel to the optical axis of the radiometers. TSIM/FY-3B had too many problems to handle the non-zero solar pointing errors. Differences in the TSI short-time variation between TSIM/FY-3B and other space instruments may be largely attributed to an incomplete correction of time-varying solar pointing errors. The non-zero and time-varying solar pointing errors are estimated based on astronomical computations, requiring a large number of auxiliary satellite data, such as the six orbital elements of the satellite. The auxiliary data are currently not included in the original Level 0 data documents. The auxiliary data need to be computed or obtained from other data documents. Matching the original Level 0 data and the auxiliary data is generally a complex and time-consuming work. It seems that the process of data matching introduces errors into the TSI data for TSIM/FY-3B that cannot be neglected.

The motivation to develop the pointing system for TSIM/FY-3C is to remove the complex correction of solar pointing errors of TSI data. A Sun window with a time of no more than

Figure 6 Pointing error in a simulation experiment of solar tracking for TSIM/FY-3C. A small solar simulator was used as a light resource. Sunlight with changing inclination was produced by controlling the attitude of a reflecting mirror. The pointing error is computed using feedbacks from the digital sun sensor.



20 minutes for each orbit could be too short for a TSI radiometer onboard a spacecraft designed for solar-dedicated space missions. However, the narrow Sun window is difficult to achieve for the solar instrument TSIM onboard a nadir spacecraft that has mainly been developed for Earth observing.

The performance of the pointing system was validated in ground experiments using a sunlight simulation system. The sunlight simulation system mainly consisted of a small solar simulator, a reflecting mirror, a coder, a displacement sensor, a displacement motor, and a rotation motor. Light generated by the solar simulator is always reflected to the digital sun sensor in the pointing system by changing the attitude of the reflecting mirror driven by the displacement motor and the rotation motor. As shown in Figure 6, the pointing error of the pointing system was smaller than 0.1 deg. The pointing system met the required pointing error tolerance.

6. Thermal Control System

TSIM/FY-3C is a delicate thermal instrument operating on a subtle thermal equilibrium. Large temperature gradients in the radiometer package are not good for the electrical substitution of the incoming sunlight, especially in the heat sink of the radiometer package. Temperature variations of the heat sink should be avoided during solar observations. Temperature drifts of the heat sink influence the process of electrical substitution inevitably and introduce thermal noises in the TSI measurements. In the system design of TSIM/FY-3C, the temperature of the heat sink is expected to be regulated to a constant reference value, with a tolerance 0.1 K to control errors. Moreover, the instrument is also kept warm by its thermal control system to survive the harsh thermal environment in space. Except for the temperature of the heat sink, the temperatures of the other instrument components are regulated to remain in predetermined scopes by the thermal control system, such as the temperatures of the external surface of the radiometer package, the temperatures of two motors in the pointing system, and the temperature of the digital sun sensor. However, temperature control tolerances for the other instrument components are much larger than for the heat sink. Several strategies are proposed for thermal control design, such as insulation of the instrument from the platform of the satellite and insulation of the pitch motor or the yaw motor

from the other components of the pointing system. The necessary electronics was separated from the sensor and the radiometer package to simplify the design and implementation of the thermal design. Feedback control methods are employed for the implementation of the thermal control system.

7. Instrument Operations

Each radiometer in TSIM/FY-3C has three basic modes: the test mode, the solar mode, and the background mode; this is nearly the same as in TSIM/FY-3B. The three basic modes are detailed in Fang *et al.* (2014) and Wang *et al.* (2015).

When the satellite is in the daytime portion and the imaged-based feedback of the solar pointing error is provided by the sun sensor, the pointing system tracks the Sun in its closed loop manner as defined in the visual servo mode. As soon as the solar pointing error is smaller than a specific predetermined value, the radiometer is enabled to operate in the solar mode. In the solar mode, the TSI is generally measured twice for each orbit. It is measured once by each radiometer during ten minutes: five minutes for the observation phase, and five minutes for the reference phase. As soon as the Sun window closes, the observing radiometers receive a command to run the test mode once, and they are immediately prepared for the next solar observation.

When the satellite is in the eclipsed portion, the radiometer runs the background mode once. The thermal background is measured once by each radiometer in each orbit. The space thermal background is measured in nearly the same way as for TSIM/FY-3B (Fang *et al.*, 2014; Wang, Li, and Fang, 2014). Unfortunately, no temperature sensors were installed in baffles, the precision apertures, and the shutters of the radiometers in TSIM/FY-3C. The thermal background of the radiometers cannot be estimated using methods used by VIRGO/SOHO or TIM/SORCE, such as the thermal modeling method (Fröhlich *et al.*, 1997), or the single value decomposition method of TIM/SORCE (Kopp, Heuerman, and Lawrence, 2005). For TSI data correction of TSIM/FY-3C, the thermal background in the daytime portion is assumed to be exactly the same as in the eclipsed portion.

According to the performance tests of the two radiometers at the beginning of the TSIM/FY-3C experiment, the radiometer AR1 is now set to perform daily measurements of the TSI in space, while the radiometer AR2 is used occasionally to investigate degradation of the AR1 cavity sensor.

8. Uncertainty Evaluation

The uncertainty evaluation method for each absolute radiometer in TSIM/FY-3C is exactly the same as in TSIM/FY-3B (Fang *et al.*, 2014; Wang, Li, and Fang, 2014). The irradiance measurement produced by each absolute radiometer is modeled as follows:

$$E = \frac{u_{\text{er}}^2 - u_{\text{eo}}^2}{RA\alpha}, \quad (2)$$

where E is the irradiance, u_{eo} and u_{er} are the heating voltages in the observation and the reference phases, respectively, R is the resistance of the heating wires for the primary cavity in the absolute radiometer, A is the area of the precision aperture, and α is the effective absorption coefficient of the primary cavity.

Table 2 Uncertainties of radiometer AR1 in TSIM/FY-3C. The experiment data for uncertainty evaluation were obtained in the ground. The radiometer runs in test mode and not in solar mode.

Parameter	Value	Relative uncertainty	Absolute uncertainty
u_{er}	8.06239 V	135 ppm	1.08564×10^{-3} V
u_{eo}	2.94259 V	369 ppm	1.08531×10^{-3} V
A	5.0290×10^{-5} m ²	471 ppm	2.370×10^{-8} m ²
R	866.70 Ω	64 ppm	0.056 Ω
α	0.9997	120 ppm	1.20×10^{-4}
E	1293.07 W m ⁻²	592 ppm	0.765055 W m ⁻²

The detailed uncertainty evaluation is omitted here for simplicity, we refer to Section 6 of Fang *et al.* (2014) for details. It should be noted here that the two absolute radiometers are commanded to work in the test mode. Details of the test mode can be found in of Fang *et al.* (2014). In test mode, the shutter is always closed. Heating voltages for the primary cavity can be repeated as many times as desired. Since experimental conditions for TSIM/FY-3C were limited to completely remove the variations of the simulating resources, external light resources were not used in the test mode to avoid their drift, for example the laser (Rubenchik, Fedoruk, and Turitsyn, 2014). The combined standard uncertainty in the irradiance for radiometer AR1 is given in Table 2.

9. Summary

A TSI instrument, TSIM/FY-3C, with a pointing system has been designed by the Changchun Institute of Optics, Fine Mechanics and Physics for the China Metrological Administration. The TSI is recorded about 26 times every day by the new TSIM. The TSI is measured with accurate solar pointing and stable temperature regulation onboard the nadir FY-3C satellite, which has mainly been developed for Earth-observing missions. The absolute radiometer AR1 operating in the routine mode provides irradiance measurements with a relative uncertainty of 592 ppm. From the in-flight results, the TSI data quality of TSIM/FY-3C has improved to a level that was not expected before, compared with the previous TSIM/FY-3A and TSIM/FY-3B. Generally speaking, this is attributed to the autonomous and accurate solar tracking and sound thermal stability of the radiometer package. The primary in-flight results of the instrument will be given in another article (Wang *et al.*, 2016). The complex corrections of the solar pointing errors needed by TSIM/FY-3A and TSIM/FY-3B are eliminated in this instrument with a pointing system, increasing the accuracy of the science data products. TSIM/FY-3C will record the decreasing trend of the TSI in Solar Cycle 24, providing more power to maintain the continuity of this series, which was initiated in 1978.

Acknowledgements This work is supported by Development Plan Project for Science and Technology of the Jilin Province (No. 20130101044JC), the Basic Research Project for application of Yunnan Province (No. 2012FD050), the Natural Science Foundation of China (No. 61077080, No. 21643006). The China Scholarship Council also provided financial support and international-travel support for this work. The authors would like to thank the staff in the Changchun Institute of Optics, Fine Mechanics and Physics, the satellite teams, and the China Metrological Administration, who were engaged in this project. The generous help from the anonymous referee is highly appreciated by the authors.

Disclosure of Potential Conflicts of Interest The authors declare that they have no conflicts of interest.

References

- BenMoussa, A., Gissot, S., Schuhle, U., Del Zanna, G., Auchere, F., Mekaoui, S., *et al.*: 2013, On-orbit degradation of solar instruments. *Solar Phys.* **288**, 389. DOI.
- Booth, M.: 2014, Adaptive optical microscopy-the ongoing quest for a perfect image. *Light Sci. Appl.* **3**, e165. DOI.
- Cetin, A., Coskun, A., Galarreta, B., Huang, M., Herman, D., *et al.*: 2014, Handheld high-throughput plasmonic biosensor using computational on-chip imaging. *Light Sci. Appl.* **3**, e122. DOI.
- Fang, W., Wang, H., Li, H., Wang, Y.: 2014, Total solar irradiance monitor for FY-3A and FY-3B satellites – Instrument design. *Solar Phys.* **289**(12), 4711. DOI.
- Fröhlich, C.: 2012, Total solar irradiance observations. *Surv. Geophys.* **33**, 453. DOI.
- Fröhlich, C., Romero, J., Roth, H., Wehrli, C., Andersen, B.N., Appourchaux, T., *et al.*: 1995, VIRGO: Experiment for helioseismology and solar irradiance monitoring. *Solar Phys.* **162**, 101. DOI.
- Fröhlich, C., Crommelynck, D.A., Wehrli, C., Anklin, M., Dewitte, S., Fichot, A., *et al.*: 1997, In-flight performance of the VIRGO solar irradiance instruments on SOHO. *Solar Phys.* **175**, 267. DOI.
- Girshovitz, P., Shaked, N.: 2014, Doubling the field of view in off-axis low-coherence interferometric imaging. *Light Sci. Appl.* **3**, e151. DOI.
- Kopp, G., Heuerman, K., Lawrence, G.: 2005, The Total Irradiance Monitor (TIM): Instrument calibration. *Solar Phys.* **230**, 111. DOI.
- Kopp, G., Lawrence, G.: 2005, The Total Irradiance Monitor (TIM): Instrument design. *Solar Phys.* **230**, 91. DOI.
- Kopp, G., Lean, J.L.: 2011, A new, lower value of total solar irradiance: Evidence and climate significance. *Geophys. Res. Lett.* **38**, L01706. DOI.
- Kopp, G., Fehlmann, A., Finsterle, W., Harber, D., Heuerman, K., Willson, R.: 2012, Total solar irradiance data record accuracy and consistency improvements. *Metrologia* **49**, S29. DOI.
- Liebetraut, P., Petsch, S., Liebeskind, J., Zappe, H.: 2013, Elastomeric lenses with tunable astigmatism. *Light Sci. Appl.* **2**, e98. DOI.
- Liu, W., Ofman, L.: 2014, Advances in observing various coronal EUV waves in the SDO era and their seismological applications (invited review). *Solar Phys.* **289**, 3233. DOI.
- Meftah, M., Dewitte, S., Irbah, A., Chevalier, A., Conscience, C., Crommelynck, D., *et al.*: 2014a, SO-VAP/Picard, a spaceborne radiometer to measure the total solar irradiance. *Solar Phys.* **289**, 1885. DOI.
- Meftah, M., Hochedez, J.F., Irbah, A., Hauchecorne, A., Boumier, P., Corbard, T., *et al.*: 2014b, Picard SODISM, a space telescope to study the Sun from the middle ultraviolet to the near infrared. *Solar Phys.* **289**, 1043. DOI.
- Mekaoui, S., Dewitte, S., Conscience, C., Chevalier, A.: 2010, Total solar irradiance absolute level from DIARAD/SOVIM on the international space station. *Adv. Space Res.* **45**, 1393. DOI.
- Memarian, M., Eleftheriades, G.: 2013, Light concentration using hetero-junctions of anisotropic low permittivity metamaterials. *Light Sci. Appl.* **2**, e114. DOI.
- Morrill, J.S., Floyd, L., McMullin, D.: 2014, Comparison of solar UV spectral irradiance from SUSIM and SORCE. *Solar Phys.* **289**, 3641. DOI.
- Rubenchik, A., Fedoruk, M., Turitsyn, S.: 2014, The effect of self-focusing on laser space-debris cleaning. *Light Sci. Appl.* **3**, e159. DOI.
- Thuillier, G., Bolsee, D., Schmidtke, G., Foujols, T., Nikutowski, B., Shapiro, A.I., *et al.*: 2014a, The solar irradiance spectrum at solar activity minimum between solar cycles 23 and 24. *Solar Phys.* **289**, 1931. DOI.
- Thuillier, G., Schmidtke, G., Erhardt, C., Nikutowski, B., Shapiro, A.I., Bolduc, C., *et al.*: 2014b, Solar spectral irradiance variability in November/December 2012: Comparison of observations by instruments on the international space station and models. *Solar Phys.* **289**, 4433. DOI.
- Wang, H., Li, H., Fang, W.: 2014, Timing parameter optimization for comparison experiments of TSIM. *Appl. Opt.* **53**, 1718. DOI.
- Wang, H., Li, H., Qi, J., Fang, W.: 2015, Total solar irradiance monitor for the FY-3B satellite – Space experiments and primary data corrections. *Solar Phys.* **290**, 645. DOI.
- Wang, H., Qi, J., Fang, W., Li, H., Wang, Y.: 2016, Initial in-flight results: The total solar irradiance monitor on the FY-3C satellite, an instrument with a pointing system. *Solar Phys.*, in press. DOI.
- Wieman, S.R., Didkovsky, L.V., Judge, D.L.: 2014, Resolving differences in absolute irradiance measurements between the SOHO/CELIAS/SEM and the SDO/EVE. *Solar Phys.* **289**, 2907. DOI.
- Witte, S., Tenner, V., Noom, D., Eikema, K.: 2014, Lensless diffractive imaging with ultra-broadband tabletop sources: From infrared to extreme-ultraviolet wavelengths. *Light Sci. Appl.* **3**, e163. DOI.
- Yang, Z., Lu, N., Shi, J., Zhang, P., Dong, C., Yang, J.: 2012, Overview of FY-3 payload and ground application system. *IEEE Trans. Geosci. Remote Sens.* **50**, 4846. DOI.
- Yu, L., Barakat, E., Sfez, T., Hvozdar, L., Francesco, J., Herzig, H.: 2014, Manipulating Bloch surface waves in 2D: A platform concept-based flat lens. *Light Sci. Appl.* **3**, e124. DOI.